International Journal of Heat and Mass Transfer 107 (2017) 168–180

Contents lists available at ScienceDirect

International Journal of Heat and Mass Transfer

journal homepage: www.elsevier.com/locate/ijhmt

Investigations into air and refrigerant side heat transfer coefficients of finned-tube CO_2 gas coolers

IDewa M.C. Santosa [a,b], Baboo L. Gowreesunker [a], Savvas A. Tassou [a,*], Konstantinos M. Tsamos [a], Yunting Ge [a]

[a] RCUK National Centre for Sustainable Energy Use in Food Chain (CSEF), Brunel University London, Uxbridge, Middlesex UB8 3PH, UK
[b] Mechanical Engineering Department, Bali State Polytechnic, Bukit Jimbaran, Kuta selatan, Badung, Bali 80361, Indonesia

ARTICLE INFO

Article history:
Received 12 July 2016
Received in revised form 27 September 2016
Accepted 2 November 2016
Available online 19 November 2016

Keywords:
CO_2 refrigeration systems
CO_2 gas coolers
Air side heat transfer coefficient
Refrigeration side heat transfer coefficient
Modelling
Computational Fluid Dynamics (CFD)

ABSTRACT

Gas coolers are heat rejection heat exchangers in vapour compression refrigeration systems that use carbon dioxide (CO_2) as refrigerant. The design of gas coolers has a significant influence on the performance of CO_2 refrigeration systems as it determines to a large extent the gas cooler/condenser pressure and the power consumption of the system. This paper investigates local refrigerant and air heat transfer coefficients in plain fin-and-tube gas cooler coils using Computational Fluid Dynamics (CFD) modelling. The aims were to provide insights into the variation of the local heat transfer rates in the coil and determine the influence of a) design enhancements such as the use of slit fins and b) to develop correlations for overall refrigerant and air heat transfer coefficients to be used in CO_2 refrigeration component and system modelling. The results from the model which was validated against experimental measurements showed that a horizontal slit on the fin between the first and second row of tubes can lead to an increase in the heat rejection rate of the gas cooler by between 6% and 8%. This in turn can lead to smaller heat exchanger heat transfer area for a given heat rejection capacity or lower high side pressure and higher efficiency for the refrigeration system. The results and heat transfer correlations developed are a valuable resource for researchers and manufacturers of CO_2 and other heat exchanger coils that experience a wide variation in refrigerant temperature during the gas cooling process.

1. Introduction

The use of Carbon dioxide (CO_2) or R-744 as a refrigerant has been increasing in recent years due to its good thermodynamic properties, zero Ozone Depletion Potential (ODP) and negligible Global Warming Potential (GWP). CO_2 has a relatively low critical temperature of 31 °C at a pressure of 72.7 bar_g. At low ambient temperatures, CO_2 refrigeration systems that reject heat to the ambient will operate subcritically, similar to conventional vapour compression refrigeration systems, whilst at high ambient temperatures they will operate supercritically with single phase heat rejection to the ambient in the heat exchanger. Because of the single phase heat rejection the heat exchanger is normally referred to as a gas cooler rather than a condenser. The temperature at which the system switches from subcritical to supercritical operation depends on the design of the heat rejection equipment, operating conditions and control strategy employed, but in the majority of cases, this transition takes place at ambient temperatures in the range between 23 °C and 27 °C [1].

Similar to air cooled condensers, air cooled gas coolers are finned tube heat exchangers with air flowing across the heat exchanger coil between the fins and tubes and the refrigerant through the tubes in a cross-counterflow arrangement [2]. The air side heat transfer coefficient is normally much lower than the refrigerant side heat transfer coefficient and thus, has a significant influence on the overall performance of the heat exchanger. For this reason, much research has been conducted to improve the air side heat transfer performance of finned tube heat exchangers [3–5]. Influencing design parameters include fin and tube materials, fin thickness, surface topology of the fins, and the spacing and dimensions of the tubes and fins, amongst others [6].

In gas coolers, during the gas cooling process, the superheated CO_2 gas undergoes a large temperature reduction and thermophysical property changes which lead to large variations in the local heat transfer coefficient. A number of researchers investigated experimentally the variation of the heat transfer coefficient of supercritical CO_2 during the cooling process. These investigations, which were aimed at developing correlations for the heat transfer

* Corresponding author.
E-mail address: savvas.tassou@brunel.ac.uk (S.A. Tassou).

http://dx.doi.org/10.1016/j.ijheatmasstransfer.2016.11.011
0017-9310/

Nomenclature

Air-off	air-side outlet heat exchanger (°C)
Air-on	air-side inlet heat exchanger (°C)
A_t	heat transfer surface area (m^2)
bar_g	pressure-gauge (Bar)
CFD	Computational Fluid Dynamics
dP	pressure difference (Pa)
c_p	specific heat capacity (J/kg-K)
h_a	air side heat transfer coefficient (W/m^2 K)
h_r	refrigerant side heat transfer coefficient (W/m^2 K)
HTC	short for heat transfer coefficient
Nu	Nusselt Number (–)
OD	outer diameter (mm)
P	static pressure (Pa)
Pr	Prandtl Number based on the film temperature (–)
$\dot{Q}$	heat rejection (W)
R-744	CO_2 refrigerant
Re_{DC}	Reynolds Number based on collar diameter (–)
T	temperature (°C)
T_{bulk}	bulk temperature (°C)
T_{film}	film temperature = $(T_w + T_{bulk})/2$
T_w	wall temperature (°C)
T_{pc}	pseudo critical temperature (°C)
u,v,w	velocity (m/s)

Greek symbols

ρ	density (kg/m^3)
Δ	change in respective parameters
μ	dynamic viscosity ($N{\cdot}s/m^2$)

Subscripts

b	bulk
ref	refrigerant (R744)
w	wall
DC	collar diameter (m)
in	inlet
out	outlet
i	inner

coefficient for single horizontal tubes, were carried out for tubes of different diameters and a range of pressures, temperatures and heat and mass fluxes [7–10]. Across the range of conditions investigated, the correlations were found to predict the heat transfer rate with a maximum error of 20% compared to those determined from experimental measurement [9]. The deviation was largely attributed to the large variation in the refrigerant properties at the pseudo-critical region. The pseudo critical region is a temperature region above the critical temperature where the specific heat capacity (c_p) and consequently the heat transfer coefficient of CO_2 reach maximum values for a given pressure [8].

Because of the large number of variables and complex heat transfer mechanisms involved, a variety of modelling approaches have been employed to investigate the heat and mass transfer performance of gas coolers. In these models, the refrigerant side heat transfer coefficients (HTCs), were invariably determined from established correlations for single phase flow and heat transfer in tubes such as those proposed by Gnielinski [16], Pitla et al. [8] and Dang and Hihara [9]. As indicated by Zilio et al. [15] these different correlations often predict similar results for CO_2 gas coolers. Ge and Cropper [11] developed a distributed model for gas coolers which takes into consideration the rapid changes in CO_2 temperature and its effect on the local HTC. The model was validated against published experimental data and was shown to predict the general trend in refrigerant temperature variation in the tubes with errors less than 2 °C. Sánchez et al. [14] developed a steady-state model for a coaxial water cooled gas-cooler which was shown to predict exit fluid temperatures with errors up to 3 °C compared with experimental data. Zilio et al. [15] obtained errors of up to 30 °C in the first few tubes of an air-cooled gas cooler where rapid cooling takes place. These errors have been attributed to the use of average values of HTCs [11], both on the refrigerant and air-side of the gas cooler.

All above investigators highlighted the importance of employing local values of HTCs in order to adequately represent the gas cooler performance. To address this problem, and more accurately account for the impact of the variation of refrigerant properties in the pseudo-critical region, two-term heat transfer correlations have been proposed for the refrigerant HTC [10]. These two terms generally refer to the density ratio and the specific heat ratio evaluated at T_b (bulk temperature) and T_w (wall temperature).

The above discussion demonstrates that the large temperature changes and wide variation of CO_2 properties in gas cooling coils require that for design optimisation much more detail knowledge of local conditions in the coil, on both the air and refrigerant sides, and their influence on heat transfer performance is necessary. Furthermore, heat transfer between higher temperature tubes at the inlet of the coil, normally in the first row of the heat exchanger, and lower temperature tubes across the continuous plate fins, reduces the overall heat transfer effectiveness of the coil. An approach that has been considered to reduce this effect is to introduce a slit in the fin between the 1st and 2nd row of tubes in the direction of refrigerant flow [1,12,13].

Because of the difficulty in obtaining sufficient information on local heat transfer conditions from measurements on full-scale gas cooler coils, most investigations to-date have been based on single tubes. Although these investigations have led to useful outputs and knowledge, they did not take into consideration the impact of local interactions between the refrigerant and air side on local and overall heat exchanger performance. To consider these interactions, this paper uses a combination of experimental investigations and modelling of two gas cooler coils to provide: i) global coil performance measurements and CO_2 refrigerant temperature distribution in the coils and ii) simulation of the heat transfer in different segments to establish local heat transfer coefficients using CFD. CFD allows data to be obtained for areas difficult to access in experimental investigations (such as within pipes or narrow sections) and avoid the physical disruptions caused by sensors. A number of investigators have used CFD to simulate finned-tube heat exchangers [21–27] but to the authors' knowledge no previous investigations on the analysis of heat transfer coefficients of CO_2 gas coolers have been reported in the literature. The results in this paper should be of benefit to researchers and designers of CO_2 gas cooler heat exchangers.

2. Experiment investigations and test facilities

The experimental investigations were carried out on two gas cooler designs: gas cooler-A (3 row-4 circuit) continuous and slit fin, Fig. 1(a) and gas cooler-B (2 row-2 circuit) continuous and slit fin, Fig. 1(b).

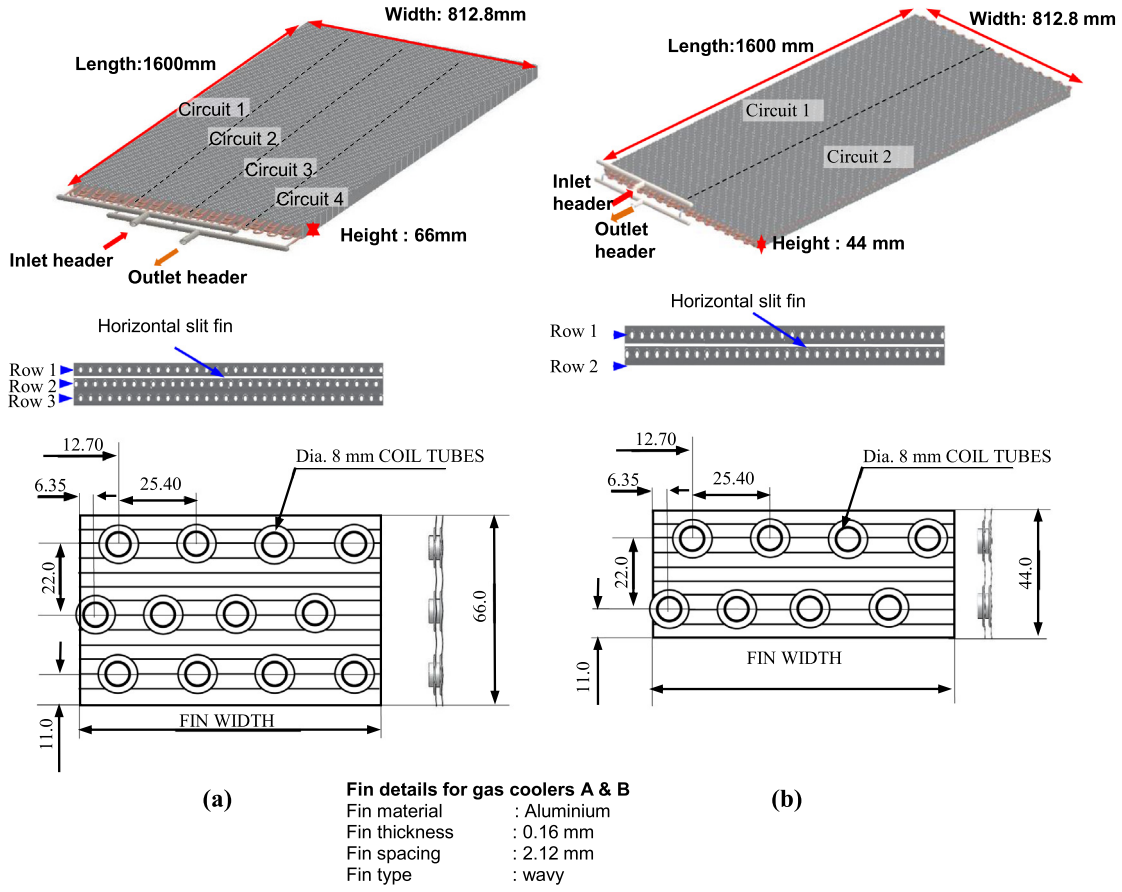

Fig. 1. Gas coolers and fin details: (a) gas cooler A, (b) gas cooler B.

2.1. Experimental test facilities

The test facilities employed are located within the Centre for Sustainable Energy Use in food chains at Brunel University London and include a CO_2 refrigeration system and gas-cooler test rig. The gas-cooler rig is shown schematically in Fig. 2(a and b). It allows for the air and refrigerant mass-flow rates and air-on temperatures on the gas cooler to be varied. Air-on temperatures were varied by regulating the air recirculation rate and modulating the electric heaters at entry to the gas cooler.

The data recorded during the tests included pressures, temperatures and mass flow rate on the refrigerant side and velocity, pressure drop and temperature on the air side. On the tube surfaces, temperatures were measured at every bend, as shown in Fig. 2 (a) and (b). The air temperature entering the gas cooler was measured at 24 points along the face of the gas cooler and at 12 points after the gas cooler. The air pressure drop across the gas cooler was measured with a differential pressure transducer KIMO CP 200, measuring range 0–80 Pa with accuracy ±1%.

Temperatures were measured with K-type thermocouples with uncertainty less than ±0.5 °C. Pressures were measured with

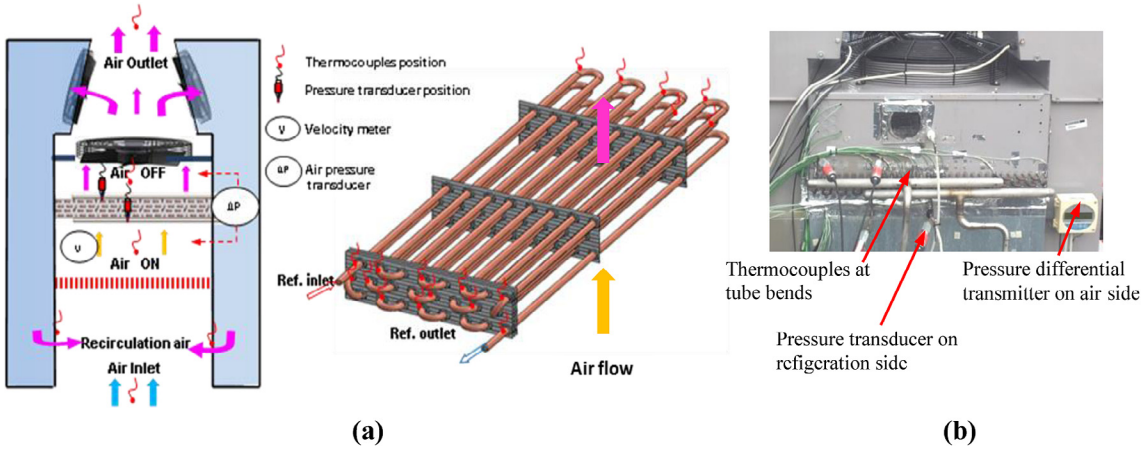

Fig. 2. Gas cooler test rig: (a) gas cooler test rig and measurement positions, (b) gas cooler photograph.

Danfoss MBS333® pressure transducers, measuring range 0–160 bar and uncertainty ±0.3%. Refrigerant mass flow rate was measured with Krohne Optimass-3000® mass flow meter with uncertainty of ±0.035%. Air velocities at the gas cooler inlet were measured with a TSI Velocicalc® Plus 8386A hot-wire anemometer with uncertainty ±3 %.

A computer based data logging system was employed and all data were logged for analysis at 20 s internals.

2.2. Test results

Tests were carried out with air velocity across the coil of 1.7 ms^{-1}, 2.0 ms^{-1}, and 2.4 ms^{-1}. The air temperature onto the coil was varied between 30 °C and 35 °C to ensure supercritical mode of operation.

The variation of the refrigerant temperature measured on the pipe surface at inlet and outlet of each pipe of the coil for different tests for the two gas coolers is shown in Fig. 3. Representative test parameters are detailed in Table 1. It can be seen from Fig. 3 that the refrigerant temperature drops exponentially as the refrigerant flows through the tubes with the largest drops in the first few tubes and very small changes in the last few tubes. It can also be seen that the drop in the refrigerant temperature is faster for Gas cooler A compared to Gas Cooler B. This is primarily due to the lower refrigerant mass flux for Gas cooler A as the flow is divided between 4 parallel sections, providing a higher heat transfer area per unit refrigerant flow, compared to the 2 parallel sections in Gas cooler B.

Considering the uncertainty of the measured variables, which include air velocity, air temperature, refrigerant (coil) temperatures and respective pressures, and assuming that the individual measurements are uncorrelated and random, the uncertainty in the calculation of heat rejection (Q) was determined to be in the range ±6.4%. These are slightly high due to the uncertainty in the temperature measurement using K-type thermocouples which was ±0.5 °C.

3. CFD modelling of gas coolers

Because of the significant complexity and computational resources required to model the entire gas cooler, the approach taken in the CFD modelling was to:

i. Assume each parallel circuit of the gas cooler to operate as separate heat exchanger connected in parallel (see Fig. 4). Measurements on the different gas cooler parallel sections showed a very similar performance and temperature variations in the gas cooler tubes, validating this assumption.
ii. Divide each gas cooler section into 5 segments along the pipe length as shown in Fig. 5(a) and assuming a linear variation of refrigerant temperature along the tube for each pipe length and each segment. It can be seen from Fig. 3 that shows the variation of refrigerant temperature between the inlet and outlet of each tube that this is also a reasonable assumption.
iii. Following from assumptions (i) and (ii), each segment of the heat exchanger was treated individually in the CFD modelling.

3.1. Governing equations

The equations governing the flow and associated heat transfer in a fluid are based on the conservation principles of mass, momentum and energy. These fundamental physical principles are expressed as the Navier-Stokes set of equations (Eqs. (1)–(3)), and because they are non-linear second-order equations, the solution procedure is complex. CFD applies and solves the discretised form of these equations for a domain, through iterations, where the pressure p, temperature T, density ρ, and velocity components u, v, w, at each grid cell can be predicted with a good degree of accuracy [27].

Continuity equation:

$$\frac{\partial \rho}{\partial t} + \frac{\partial}{\partial x_j}(\rho u_j) = S_M \tag{1}$$

Momentum equation:

$$\frac{\partial}{\partial t}(\rho u_j) + \frac{\partial}{\partial x_j}(\rho u_i u_j) = -\frac{\partial}{\partial x_j}(P) + \frac{\partial}{\partial x_j}(\bar{\tau}) + \rho g_j + F_j \tag{2}$$

Energy Equation:

$$\frac{\partial}{\partial t}(\rho H) = -\frac{\partial}{\partial x_j}(\rho u_j c_p T) + \frac{\partial}{\partial x_j}\left[\lambda \frac{\partial T}{\partial x_j}\right] + S_E \tag{3}$$

One of the challenging aspects of modelling fluid flows in different scenarios is the distinction of flow regimes. Fluid flows comprise different turbulence regimes, depending on the geometry of

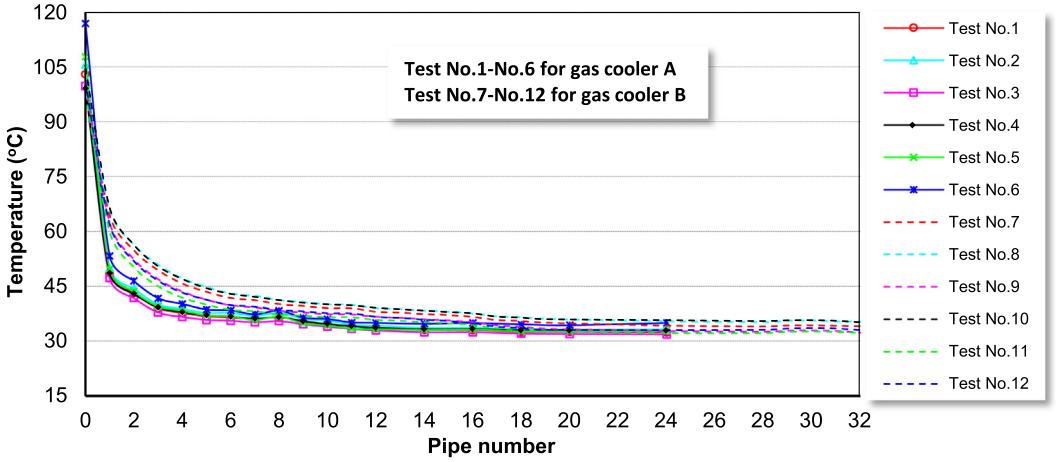

Fig. 3. Representative test results of coil tube temperature profile. (Experimental conditions similar to No.1 – No.12 in Table 1).

Table 1
Representative test results for gas coolers A and B with slit fins.

Test	v (m/s)	$T_{air\ on}$ (°C)	P_{ref_in} (Bar-g)	T_{ref_in} (°C)	$\dot{m}_{ref}$ (kg/s)	$T_{air\ off}$ (°C)	T_{ref_out} (°C)	dP_{air} (Pa)	Q (kW)	±Q (kW)
Gas cooler A										
Test No. 1	1.7	32.2	82.8	102.9	0.041	36.2	32.3	24.1	9.4	0.60
Test No. 2	1.7	32.8	85.1	105.5	0.042	36.9	33.2	26.6	9.6	0.62
Test No. 3	2.0	31.8	81.4	99.7	0.039	35.0	31.8	33.0	8.9	0.57
Test No. 4	2.0	32.8	84.2	99.2	0.040	35.9	32.8	34.2	8.9	0.57
Test No. 5	2.4	32.4	85.4	107.7	0.038	35.1	32.8	39.5	9.0	0.58
Test No. 6	2.4	34.3	86.6	116.8	0.041	37.2	34.9	41.4	9.6	0.61
Gas cooler B										
Test No. 7	1.7	33.7	84.9	100.3	0.042	37.6	34.0	13.7	8.9	0.56
Test No. 8	1.7	35.1	86.3	100.8	0.038	38.7	35.3	13.9	8.2	0.52
Test No. 9	2.0	32.6	82.5	100.2	0.039	35.7	32.3	21.5	8.6	0.55
Test No. 10	2.0	35.2	86.5	104.6	0.043	38.5	35.0	25.6	9.2	0.58
Test No. 11	2.4	32.0	81.5	97.6	0.042	34.9	32.2	27.6	9.2	0.59
Test No. 12	2.4	33.0	83.9	101.3	0.042	35.9	33.0	27.6	9.3	0.60

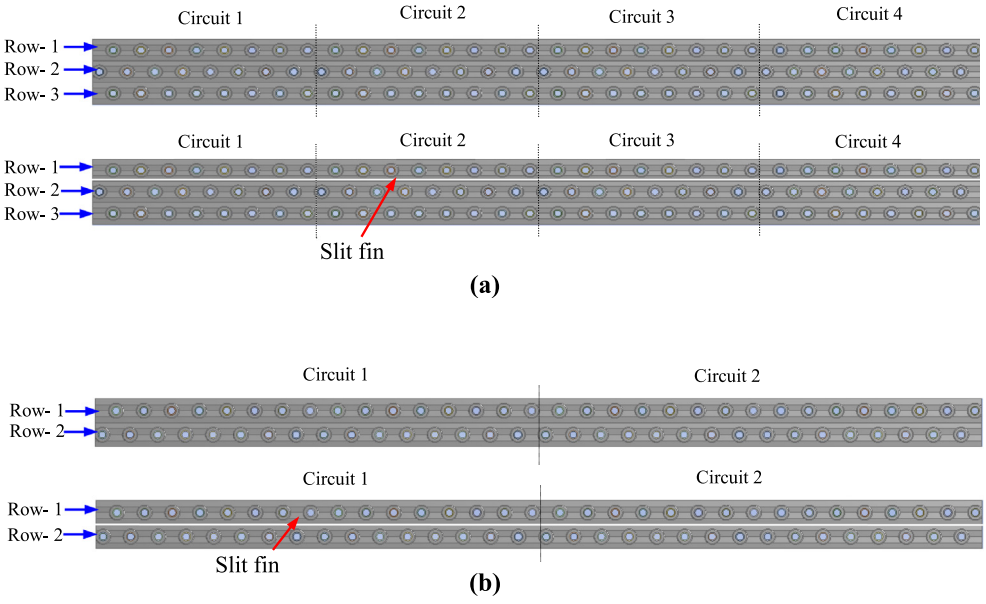

Fig. 4. CFD geometry of gas coolers: (a) gas cooler A with continuous and slit fin, (b) gas cooler B with continuous and slit fin.

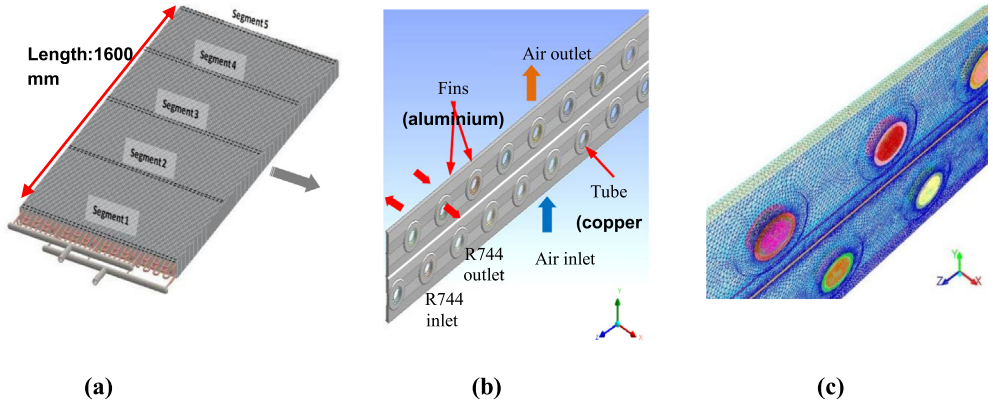

Fig. 5. CFD boundary conditions and meshing: (a) segment position along gas cooler, (b) model geometry and boundary conditions, and (c) meshing of geometry.

the heat exchanger and surface topologies. High Reynolds number flows provide higher heat transfer rates, compared to lower Reynolds flows, and is therefore important that the model captures the turbulence aspect of the flow. The following section describes the turbulence models used in previous air-flow studies.

3.2. Turbulence models

The application of CFD in various heat-exchanger design and optimisation studies has in most cases employed the *k-ε* turbulence models [21]. Amongst these, the standard *k-ε*, *SST*, *realizable*

k-ε and *RNG k-ε* models have been the most popular, but their choice has been dependent on the specific heat exchanger being investigated. Singh et al. [23], used CFD to model the steady-state air-side heat transfer of a finned tube heat exchanger. The numerical results, using different turbulence models were compared with experimental data and the *Realizable k-ε* model was found to produce the best predictions with a maximum error of 4% [23]. Sun and Zhang [25] also employed the *Realizable k-ε* model to evaluate the performance of elliptical finned-tube heat exchangers. Validation of the CFD model was performed on the prediction of heat transfer coefficients in the heat-exchanger, and maximum error was found to be 4.7%. The *RNG k-ε* model was employed by Bilirgen et al. [26]. to investigate the effects of different fin thickness, height, material type and Reynolds number of the air-flow on the performance of finned tube heat exchangers where the air-flow was assumed to be incompressible and steady-state [26]. The *RNG k-ε* was also reported to give accurate predictions for the velocity field, the turbulent kinetic energy and the recirculation length of flows in helically finned tubes [24].

In general, there is no universal turbulence model for heat-exchangers, because of the wide variation of geometries and flow regimes encountered. As part of this study, different turbulence models were investigated, and their validity compared against experimental data, in order to determine which turbulence model is more suitable for the particular heat exchanger design employed.

3.3. CFD boundary conditions and meshing

The CFD model developed was for finned copper tubes of 8 mm outer-diameter and 0.68 mm wall thickness, and wavy aluminium fins of 0.16 mm thickness and 2.12 mm air gap between the fins. Simulation was performed for 5 segments along the tubes of the gas cooler, at 0 m; 0.4 m; 0.8 m; 1.2 m; and 1.6 m from the inlet of the heat exchanger as shown in Fig. 5(a).

Since the fins are only 0.16 mm thick, the meshing of such a thin surface was found to be problematic in terms of the mesh type and size, especially when considered in the context of the overall gas cooler domain. Hence, the concept of thin-wall shell conduction available in ANSYS FLUENT® [28] was employed. This refers to the simplification of the material heat transfer discretisation to a single node within the thickness, therefore avoiding meshing to very small levels. It allows for a more convenient representation of heat conduction within the fin, for the modelling of finned-tube heat exchangers as suggested by ANSYS FLUENT® [28].

The boundary conditions used in this study with reference to Fig. 5(b) were defined as follows:

- The refrigerant inlet mass flow rate and temperature at inlet to each tube were input to the model. A linear variation of temperature was assumed for the tube segments as shown in Fig. 3.
- The air enters between two fins (y-direction), at a constant velocity and temperature obtained from the experimental tests (see Table 1).
- The fins and fin collar were modelled as thin-walls.
- The thermo-physical properties (density, viscosity, specific heat capacity, thermal conductivity) of air and refrigerant (R744) as a function of temperature and pressure were obtained using the Engineering Equation Solver (EES) software [29]. These were incorporated in FLUENT® using the piecewise-linear formulation.
- The thermo-physical properties of copper and aluminium were obtained from the FLUENT® database.

The model was meshed using tetrahedral type elements and three different numbers of cells were tested with respect to the residual convergence of the models. Using the coarse (1.2 million cells) and medium (3.2 million cells) grids, the convergence of residuals reached minimum at 10^{-4} for continuity, 10^{-7} for energy, 10^{-3} for x, y and z, 10^{-3} for turbulence, whilst the fine grid (4.3 million cells) was found to have residuals in the order of 10^{-5}, 10^{-8}, 10^{-6} and 10^{-4}, respectively. Following the satisfactory residuals obtained from the fine grid, the latter was used for subsequent simulations, at the expense of higher computing time compared to the other mesh sizes. The final mesh is shown in Fig. 5(c), whereby high grid densities have been used in all areas where high temperature gradients were more likely to occur at the fin collars and in the proximity of the tubes.

In addition to having simulations with adequate convergence criteria, the turbulence model influences the final simulation results [21]. In this regard, different turbulence models available in the FLUENT® software were investigated. These turbulence models included: Standard, Realizable and Renormalisation Group *(RNG) k-ε* model; Standard and *SST k-ω* models; and the laminar model. The numerical results with different turbulence models were compared with experimental data, in order to determine the validity of each turbulence model as explained in following section.

3.4. Validation of the CFD model against experimental results

The validation study consisted, firstly of determining the performance of the turbulence model, and secondly of obtaining the errors of the model for different test conditions. The validation studies were conducted with respect to air-off temperature for different experimental test conditions. The air-off temperature was obtained from the mean values of the five simulated segments for each experimental condition. The *k-ε* turbulence models were found to give better performance with absolute errors in air-off temperatures as follows: *Standard k-ε*: 0.25 K, *RNG k-ε*: 0.08 K, *Realizable k-ε*: 0.07 K. The *k-ω* models showed slightly worse performance (*Standard k-ω*: 0.31 K, and *SST k-ω*: 0.33 K, compared to the *k-ε* models. The laminar model produced a 1.31 K error. As the *Realizable k-ε* model showed the best performance, it was adopted for subsequent simulations.

4. Air and refrigeration side-heat transfer coefficient calculation methodology

As alluded to in section 1, the heat transfer coefficients of the gas cooler are crucial in determining its overall performance. Unlike previous work, this study does not impose heat transfer correlations on the model, but rather, these are calculated implicitly in the model. Hence, this section depicts the effectiveness of CFD to determine the heat transfer coefficients.

The air side heat transfer coefficients h_a, in each segment for the tube bundles/fin walls are deduced from the heat-transfer rate Q, the heat-transfer surface area $A_t = A_{collar} + A_{fins}$, wall temperatures $T_w = (T_{collar} + T_{fin})/2$ and air bulk temperature $T_b = (T_{in} + T_{out})/2$. Eq. (4) was used for the calculation of the air-side heat transfer coefficient (h_a). This equation format was chosen mainly to adhere with the formulation used in the literature [5].

$$h_a = \frac{\dot{Q}}{(A_t)(T_w - T_b)} \quad (W/m^2K) \tag{4}$$

$$\dot{Q} = \dot{m}_{air} \cdot \Delta h_{air} \quad (W), \tag{5}$$

where $\dot{m}_{air}$ is air mass flow rate and Δh_{air} is enthalpy difference between air inlet and outlet

Furthermore, the refrigerant-side heat transfer coefficient (h_r) was determined for individual segments using Eq. (6) as follows:

$$h_r = \frac{Heat\ flux_{ref}\left(\frac{W}{m^2}\right)}{(T_{w,i} - T_b)K} \quad (6)$$

where, the heat flux (W/m^2) is the heat flux from the refrigerant to the inner wall surface of the copper tube, $T_{w,i}$ (°C) is the temperature of the inner pipe surface (copper), T_b (°C) is the mean refrigerant pipe inlet and outlet temperatures for each segment.

Fig. 6 shows the CFD results for temperature and velocity contours for a segment. It shows the wall temperature contours, air flow path-line, and the refrigerant flow vectors of pipe-1 and pipe-2 of the gas cooler, where the refrigerant heat fluxes, wall temperatures, refrigerant and air outlet temperatures were calculated from the model. Based on these results, the air and refrigerant side heat transfer coefficients were calculated for individual segments for the entire gas cooler using Eqs. (4) and (6), respectively.

The CFD results for the gas cooler segments of the two gas coolers investigated are shown in Figs. 7(a) and (b). Gas cooler A (24 tubes, 3 rows, 4 circuits) is shown in Fig. 8(a); and gas cooler B (32 tubes, 2 rows, 2 circuits) is shown in Fig. 8(b). The investigation of the heat transfer coefficients was performed for one circuit and assumed to be similar for the other circuits, due to the similarities in temperatures in the other circuits observed from the test results.

5. Results and discussion

5.1. Air flow characteristics in gas cooler fin and tube passages

The flow characteristics in the heat exchanger flow passages are influenced by the tube and fin structures and arrangement. Fig. 9 presents the flow characteristics at each row of the gas coolers. As expected, each row has a stagnant area at the rear of each tube in the direction of air flow which reduces heat transfer. Increasing turbulence and reducing this stagnant area will improve the air side heat transfer coefficient [3].

5.2. Air side heat transfer coefficient (h_a) profile in segments

The variation of the air side heat transfer coefficient in one circuit of gas cooler A with continuous fins is shown in Fig. 9(a). From Eq. (4), the air side heat transfer is a function of the heat transfer in the domain between refrigerant and air and the temperature difference between the wall, tube and fins, and the air. It can be seen that in the third row, h_a, is fairly constant at around 150 W/m^{2}K, due to the constant temperature of both air (air on temperature) and refrigerant as can be seen from Fig. 3. In the 2nd row, h_a increases until pipe 12 to around 175 W/m^{2}K, and then drops down to just below 100 W/m^{2}K at the start of the first row, pipe 8, before rising again slowly just above 100 W/m^{2}K in pipe 1. These variations are a function of the relative influence between the rapid drop in the refrigerant temperature from pipe 1 to pipe 8 and the difference in temperature between the pipe and fin and the bulk air temperature.

The variation of the air side heat transfer coefficient for gas cooler A with horizontal slit fin is shown in Fig. 9(b). It can be seen that the slit has a significant influence on the air side heat transfer of the second (middle) row of tubes. This is due to the influence of the slit on reducing the heat transfer across the fin between the first and second row of tubes. Lower fin and tube temperatures lead to higher air side heat transfer coefficients.

The air side heat transfer coefficient, h_a, for gas cooler B, continuous fin, is shown in Fig. 9(c). It can be seen that (h_a) in the second row of tubes, 17–32, first increases from around 80 W/m^{2}K pipe 32, to around 110 W/m^{2}K pipe 24 before dropping back to 85 W/m^{2}K pipe 16. The drop is due to the higher pipe and fin temperatures in this region and heat transfer from first and second row of tubes across the fin. In the first row of tubes, pipe 17, h_a begins to rise, reaching maximum of around 100 W/m^{2}K at pipe 14 before dropping back to 80 W/m^{2}K at pipe 1 due to the very high tube and fin temperatures at refrigerant entry to the gas cooler.

Fig. 9(d) shows the effect of the slit fin. It can be seen that h_a in the second (bottom) row remains relatively constant dropping slightly from 115 W/m^{2}K at row 32 to around 110 W/m^{2}K at row 17 due to the higher pipe and fin temperatures in this region. In the first row of tubes, pipe 16, h_a, has a low value of 80 W/m^{2}K, rising to 110 W/m^{2}K at pipe 5 before dropping back to 100 W/m^{2}K at pipe 1, the refrigerant entry to the heat exchanger.

5.3. Correlation of average air side heat transfer (h_a) with Reynolds Number (Re)

Based on the results of the local and average air side heat transfer coefficients, correlations were developed for the determination of the air side heat transfer coefficient of gas coolers based on the approach proposed by Chang and Kim [20], relating the Nusselt number to the Reynolds and Prandtl numbers.

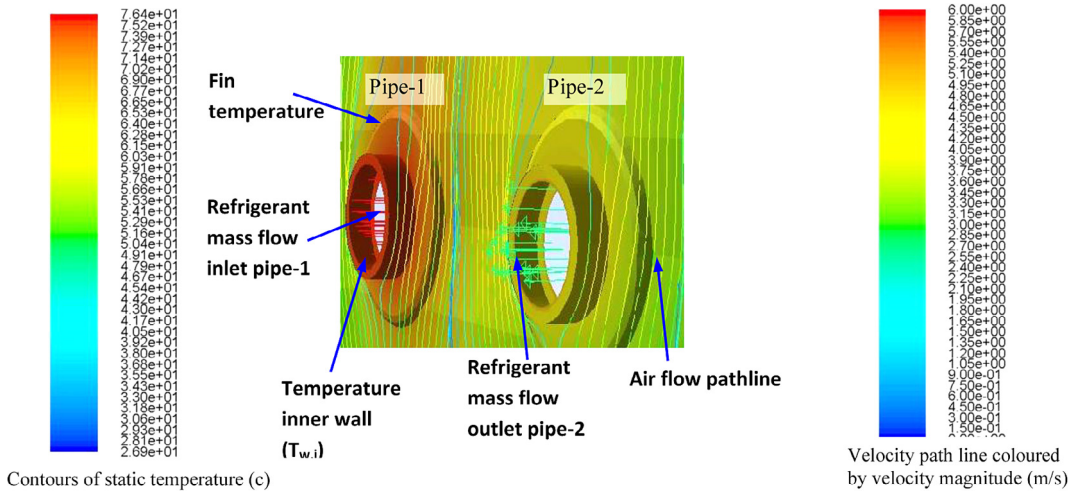

Fig. 6. CFD post processing at a segment of fined–tube heat exchanger.

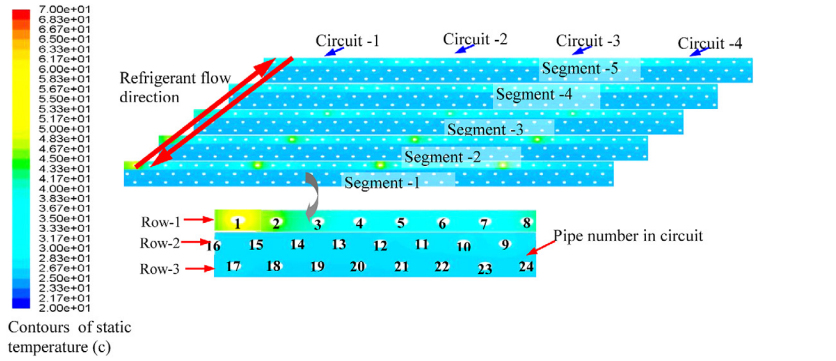

Fig. 7. Gas cooler segment CFD results: (a) gas cooler A, (b) gas cooler B.

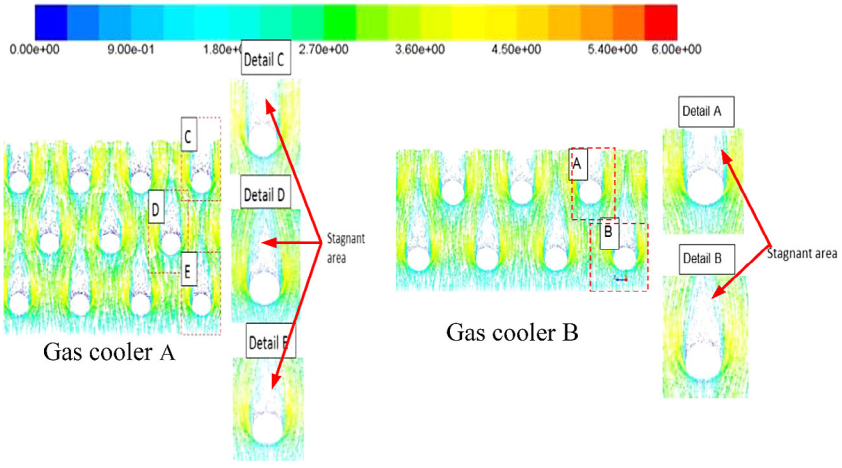

Fig. 8. Air flow characteristic of gas coolers A and B (Air inlet velocity = 1.7 m/s).

The calculation of the local Reynolds Number was based on the fin collar diameter (Dc) for simplicity and the fact that this dimension has the greatest influence on turbulence in the heat exchanger [2,17–20], as illustrated in Eq. (7).

$$\mathrm{Re}_{DC} = \frac{inertia\ \ forces}{viscous\ \ forces} = \frac{\rho u^2 D_C^2}{\mu u D_c} = \frac{\rho u D_C}{\mu} \tag{7}$$

The values of the thermo-physical properties of air were obtained at the film temperature (T_{film}), i.e. the average of T_{bulk} and T_w, and these values were obtained from the CFD results.

Fig. 10 shows the average heat transfer coefficients, based on 12 points, of gas cooler A with continuous and slit fin with respect to Reynolds Number (Re_{DC}).

The respective correlations for the average air-side heat transfer coefficients for the continuous and slit fin of gas cooler A were found to be:

- Gas cooler A continuous fin design:

$$Nu_{DC} = 4\ \mathrm{Re}_{DC}^{0.356}\mathrm{Pr}^{1/3} \tag{8}$$

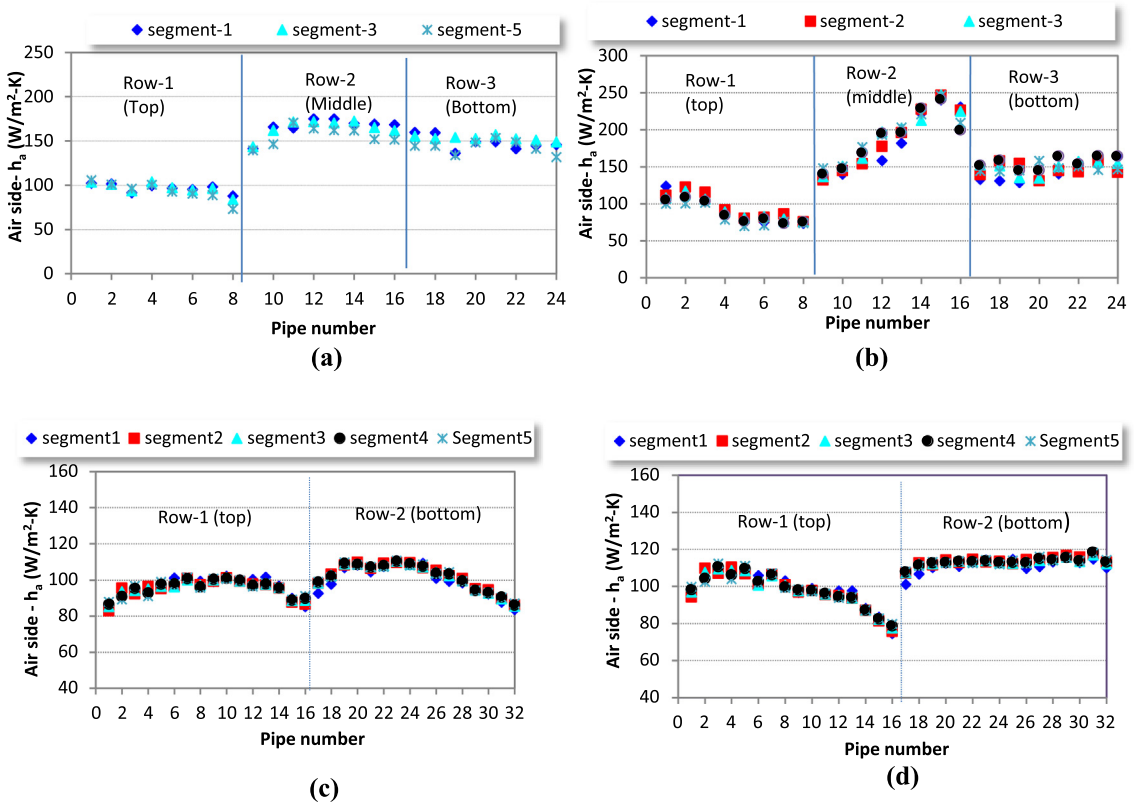

Fig. 9. Air side heat transfer coefficient at segments: (a) gas cooler A with continuous fin, (b) gas cooler A with slit fin, (c) gas cooler B with continuous fin, and (d) gas cooler B with slit fin.

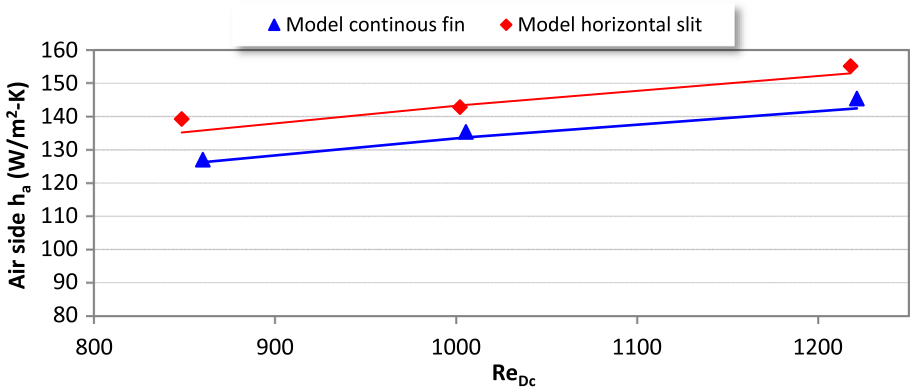

Fig. 10. Variation of average h_a with Reynold Number of gas cooler A.

Regression coefficient (R^2) = 0.998.

- Gas cooler A with horizontal slit fin design:

$$Nu_{DC} = 4\ Re_{DC}^{0.366} Pr^{1/3} \quad (9)$$

Regression coefficient (R^2) = 0.957.

Fig. 11 shows the average heat transfer coefficients of gas cooler B with the slit and continuous fin designs with respect to Reynolds Number (Re_{DC}). The respective correlations for the average air-side heat transfer coefficients for the slit and continuous fins of gas cooler B were found to be:

- Gas cooler B with continuous fin design:

$$Nu_{DC} = 4\ Re_{DC}^{0.331} Pr^{1/3} \quad (10)$$

Regression coefficient (R^2) = 0.990.

- Gas cooler B with horizontal slit fin design:

$$Nu_{DC} = 4\ Re_{DC}^{0.339} Pr^{1/3} \quad (11)$$

Regression coefficient (R^2) = 0.992.

The correlations indicate that as Re_{Dc} increases, the heat-transfer coefficients (h_a) also increase. The heat-transfer coefficients of gas cooler A were found to vary between 139–155 W/m^{2}K for the horizontal slit fin and 126–145 W/m^{2}K for continuous fin design. The heat-transfer coefficients of gas cooler B were found to vary between 95–127 W/m^{2}K for the slit fin design and 88–120 W/m^{2}K for the continuous fin design.

The higher average heat transfer coefficient for the slit fin design can be attributed to the fact that the conduction effect from

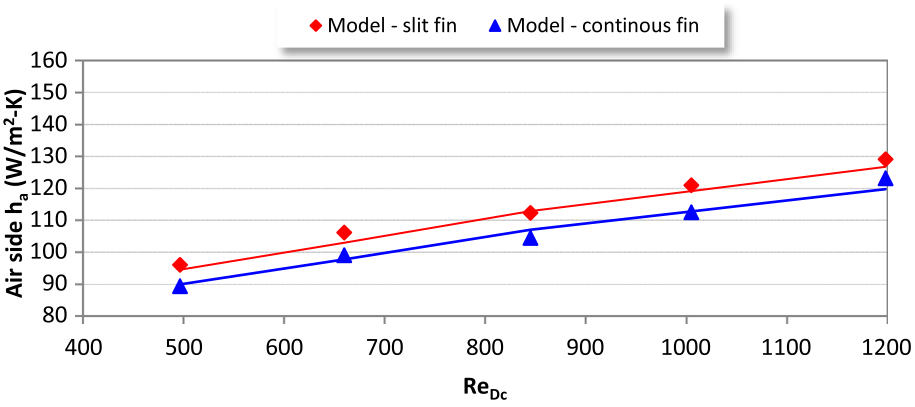

Fig. 11. Variation of average h_a with Reynold Number of gas cooler B.

the hottest pipe through the fin is mitigated by the slit. The improvement in heat transfer coefficient with the slit fin configuration leads to higher performance for the gas cooler. Compared with the continuous fin, the horizontal slit fin improved h_a by approximately 6–8%.

The CFD results from gas cooler B were compared with the limited number of previous studies (Wen and Ho [5] and Chang and Kim [20]). However, the specifications of the gas coolers were slightly different as shown in Table 2. The trends in Fig 12 (a) and (b) show that despite the different design specifications the trends in variation of the air-side heat transfer coefficient are similar demonstrating the validity of the results obtained in the present study. Comparisons of results with those of Chang and Kim were carried out for air relative humidity of 60%.

5.4. Refrigerant side heat transfer coefficient (h_r)

The investigation of the refrigerant side heat transfer coefficient (h_r) was carried out for different mass flow rates and bulk temperatures for gas coolers A and B. The average mass flow rate of CO_2 in each circuit of the gas cooler was 0.0095 kg/s for gas cooler A and 0.0195 kg/s for gas cooler B. The inner pipe diameter for the two gas coolers was the same, at 6.32 mm, giving a mass flux (G) of 310 kg/s-m^2 for gas cooler A and 620 kg/s-m^2 for gas cooler B.

The variation of h_r of gas cooler A with bulk temperature is shown in Fig. 13(a) for average pressure in the gas cooler of 83 bar$_g$ and mass flow rate of 0.0095 kg/s. The different colours represent the different segments along the length of the coil. Fig. 13(a) also shows the variation of specific heat, c_p, for the refrigerant and the heat transfer coefficient calculated from the correlation of Oh and Son [10]. It can be seen that the variation of h_r follows closely the variation of c_p, starting from a low value at the high refrigerant temperatures and rising with decreasing temperatures, reaching maximum of 2200 W/m^{2}K at 40 °C which corresponds to the temperature of maximum specific heat for the refrigerant [7–10].

For gas cooler B, the mass flow rate in the circuits is approximately double that of gas cooler A due to the smaller number of circuits. Fig. 13(b) shows the refrigerant side heat transfer coefficient (h_r) of gas cooler B as a function of bulk temperature (T_{bulk}) for refrigerant pressure of 82 bar$_g$ and refrigerant mass flow rate of 0.0195 kg/s, (G = 620 kg/s-m^2). It can be seen that the maximum h_r is approximately 3600 W/m^2-K at approximately bulk temperatures of 40 °C. The lowest h_r of 1700 W/m^2-K occurs at the highest bulk temperature of 98 °C.The two-term correlation by Oh and Son [10] is given in Eqs.(12) and (13).

$$Nu_b = 0.023 Re_b^{0.6} \cdot Pr_b^{3.2} \cdot \left(\frac{\rho_b}{\rho_w}\right)^{3.7} \cdot \left(\frac{C_{p,b}}{C_{p,w}}\right)^{-4.6} \quad \text{for} \quad T_b/T_{pc} \leqslant 1 \tag{12}$$

$$Nu_b = 0.023 Re_b^{0.7} \cdot Pr_b^{2.5} \cdot \left(\frac{C_{p,b}}{C_{p,w}}\right)^{-3.5} \quad \text{for } T_b/T_{pc} > 1 \tag{13}$$

where $C_{p,b}$ and $C_{p,w}$ indicate the specific heat evaluated at T_b and T_w, respectively and T_{pc} is temperature of maximum $C_{p,b}$.

It can be seen that for both gas coolers the refrigerant heat transfer coefficients obtained from the CFD simulations correlate well with those predicted using the correlations by Oh and Son. The greatest difference occurs in the pseudocritical region where the specific heat reaches maximum values. In this region the Oh and Son correlations predict higher values, maximum difference 18% for gas cooler A, and 12% higher for gas cooler B than the CD results. The differences are very likely to be due to the rapid variation of c_p in this region and uncertainties in both the experimental investigations and CFD modelling to accurately capture the effects of these variations.

Figs. 14(a) and (b) show the h_r profile in gas coolers A and B respectively, and its variation along the pipes of each section. For gas cooler A, the refrigerant temperature drops very rapidly from 105 °C to 50 °C in pipe 1 and the heat transfer coefficient increases from around 1000 W/m^2 K to a maximum of 2000 W/m^2 K due to the large drop in temperature and increase in the specific heat. Thereafter, h_r remains fairly constant in the range between 1700 and 2000 W/m^2 K. The small variations along the pipes are due to the variations in the refrigerant and pipe wall temperatures along the 3 rows of the gas cooler.

Table 2
Gas cooler specification for CFD model and from Wen and Ho [5] and Chang and Kim [20].

Specification	CFD Model	Experiment of Wen and Ho[5]	Chang and Kim [20]
Fin type	Wavy fin	Wavy fin	Louver
Number of rows	2	2	2
Tube outer diameter	8 mm	10.3 mm	7 mm
Inside diameter	6.32 mm	10.1 mm	6.4 mm
Fin spacing	2.11 mm	2.54 mm	–
Fin thickness	0.16 mm	0.12 mm	–
Number of pipes in circuit	32	20	–
Working fluid	CO_2	water	CO_2
Tube vertical spacing	22 mm	22 mm	–
Tube horizontal spacing	25.4 mm	24 mm	–

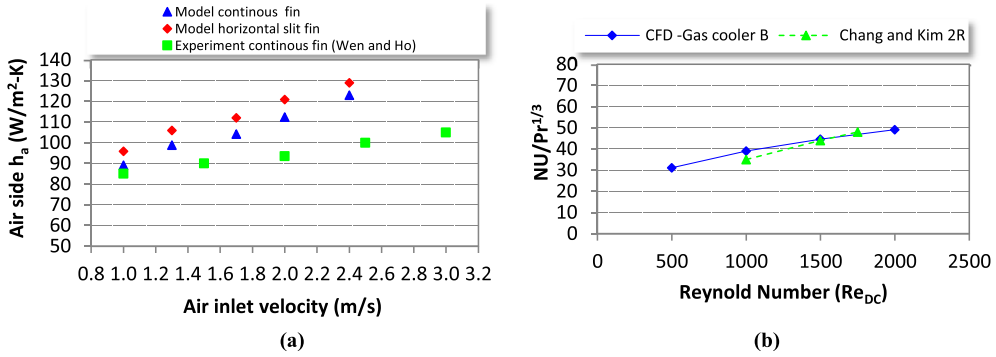

Fig. 12. Comparison the CFD result with other studies: (a) Wen and Ho [5], (b) Chang and Kim[20].

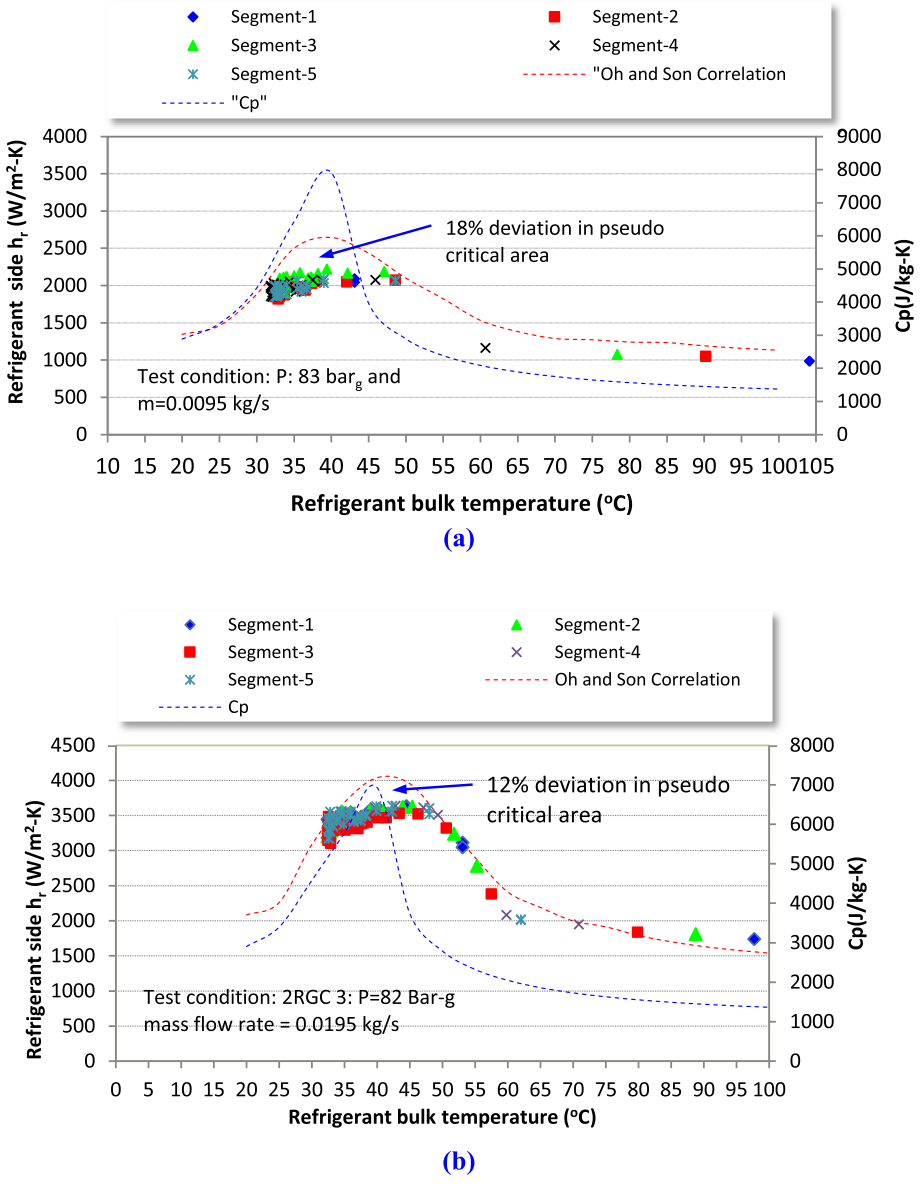

Fig. 13. Variation of refrigerant side heat transfer coefficient (h_r) with bulk temperature and comparison with correlation by Ho and Son [10]: (a) gas cooler A, (b) gas cooler B.

For gas cooler B, the heat transfer coefficient is much higher than gas cooler A due to the much higher mass flux in the pipes. Gas cooler A has 4 parallel sections whilst gas cooler B only has 2 sections, resulting in much higher mass flux but also higher pressure drop. The heat transfer coefficient in Gas cooler B increases from around 1800 W/m^2 K in pipe 1 where the refrigerant temper-

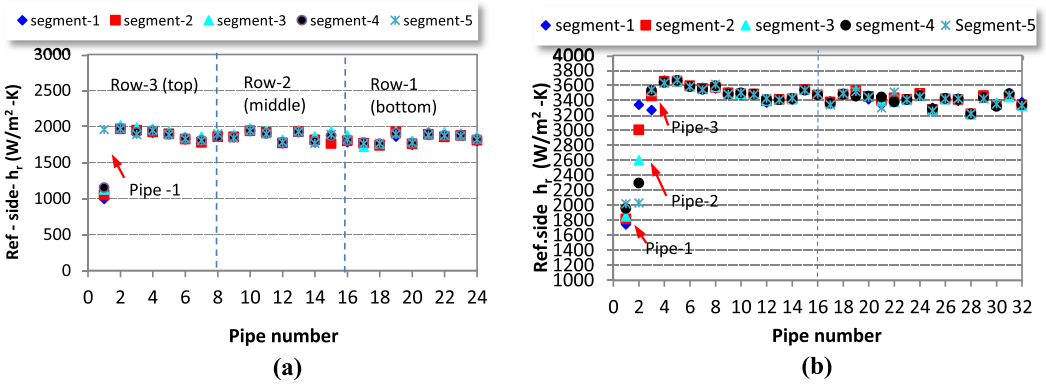

Fig. 14. Variation of h_r at segment: (a) gas cooler A, (b) gas cooler B.

ature at inlet is 98 °C to a maximum of 3700 W/m^2 K at pipe 4 where the temperature drops to around 45 °C. After this h_r drops slowly to 3400 W/m^2 K at pipe 8 and then remains fairly constant to the end of the heat exchanger.

6. Conclusions

A Computational Fluid Dynamics (CFD) model was developed and used to study the air and refrigerant side heat transfer coefficients in CO_2 gas coolers. The model was validated against experimental data with respect to heat rejection rate and air-off temperature. The *Realizable k-ε* turbulence model was found to produce best results with a mean absolute error in the prediction of the air off temperature of the gas cooler coil of 0.07 K. In summary,

1. CFD modelling was found to be able to adequately represent the heat transfer characteristics of the gas cooler and be an effective simulation tool for the determination of local air and refrigerant-side heat transfer coefficients in the coil.
2. For the air side heat transfer coefficients evaluations were performed for both local and mean heat exchanger heat transfer coefficient values and correlations were developed for the determination of these heat transfer coefficients as functions of the Prandtl (Pr) and Reynolds (Re) numbers.
3. Modelling and experimental results showed that a slit-fin design for the gas cooler coil will enhance heat transfer by reducing heat conduction between the top and second row of tubes in the heat exchanger across the fins. This improves the heat rejection rate of the heat exchanger by between 6% and 8% which can lead to lower gas cooler pressures and higher efficiency for the refrigeration system and/or smaller size for the coil.
4. The refrigerant heat transfer coefficient was investigated for different segments of the gas cooler. It was found that the trend in the variation of the refrigerant side heat transfer coefficient followed closely the variation of the specific heat of the refrigerant with temperature. This variation can be as high as 200% along the pipe length of the gas cooler.
5. The results in the paper are a valuable resource for both researchers and manufacturers engaged in the design and manufacture of gas coolers for CO_2 refrigeration applications.

Acknowledgements

This study was supported by the RCUK National Centre for Sustainable Energy use in Food chains (CSEF) of the Research Councils UK Energy programme, Grant No: EP/K011820/1, GEA Searle, now Kevlion, and Directorate General for Higher Education-DIKTI–Indonesian Government for a PhD scholarship. The authors wish to acknowledge the cash and in-kind contributions of these organisations, particularly Simon Jones and Nick Atkins of Kevlion, for their technical input throughout the project.

References

[1] ID.M.C. Santosa, IN. Suamir, Y.T. Ge, K. Tsamos, S.A.Tassou. Modelling and analysis of CO2 gas coolers for commercial refrigeration applications, in: Proc. 2nd Conference on Sustainability and the Cold Chain, Paris, 2013. ISBN: 978-2-913149-97-7. paper S12-P2.
[2] Y.C. Liu, S. Wongwises, W.J. Chang, C.C. Wang, Air side performance of fin-and-tube heat exchangers in dehumidifying conditions – data with larger diameter, Int. J. Heat Mass Transfer 53 (2010) 1603–1608.
[3] X. Du, L. Feng, L. Li, L. Yang, Y. Yang, Heat transfer enhancement of wavy finned flat tube by punched longitudinal vortex generators, Int. J. Heat Mass Transfer 75 (2014) 368–380.
[4] M. Lee, Y. Kim, H. Lee, Y. Kim, Air-side heat transfer characteristics of flat plate finned-tube heat exchangers with large fin pitches under frosting conditions, Int. J. Heat Mass Transfer 53 (2010) 2655–2661.
[5] M.Y. Wen, C.Y. Ho, Heat-transfer enhancement in fin-and-tube heat exchanger with improved fin, Appl. Therm. Eng. 29 (2009) 1050–1057.
[6] R.K. Shah, D.P. Sekulic, Fundamentals of Heat Exchanger Design, John Wiley & Sons, New Jersey, 2003, ISBN: 0-471-32171-0.
[7] R. Yun, Y. Hwang, R. Radermacher, Convective gas cooling heat transfer and pressure drop characteristics of supercritical CO_2/oil mixture in a minichannel tube, Int. J. Heat Mass Transfer 50 (2007) 4796–4804.
[8] S.S. Pitla, E.A. Groll, S. Ramadhyani, New correlation to predict the heat transfer coefficient during in-tube cooling of turbulent supercritical CO_2, Int. J. Refrig. 25 (2002) 887–895.
[9] C. Dang, E. Hihara, In-tube cooling heat transfer of supercritical carbon dioxide. Part 1. Experimental measurement, Int. J. Refrig. 27 (2004) 736–747.
[10] H.K. Oh, C.H. Son, New correlation to predict the heat transfer coefficient in-tube cooling of supercritical CO_2 in horizontal macro-tube, Exp. Thermal Fluid Sci. 34 (2010) 1230–1241.
[11] Y.T. Ge, R.T. Croper, Simulation and performance evaluation of finned-tube CO_2 gas coolers for refrigeration systems, Appl. Therm. Eng. 29 (2009) 957–965.
[12] C.Y. Park, P. Hrnjak, Effect of heat conduction through the fins of a microchannel serpentine gas cooler of transcritical CO_2 system, Int. J. Refrig. 30 (2007) 389–397.
[13] V. Singh, V. Aute, R. Radermacher, Investigation of effect of cut fins on carbon dioxide gas cooler performance, HVAC&R Res. 16 (4) (2010).
[14] D. Sánchez, R. Cabello, R. Llopis, E. Torrella, Development and validation of a finite element model for water – CO_2 coaxial gas-coolers, Appl. Energy 93 (2012) 637–647.
[15] C. Zilio, L. Cecchinato, M. Corradi, G. Schiochet, An assessment of heat transfer through fins in a fin-and-tube gas cooler for transcritical carbon dioxide cycles, HVAC&R Res. 13 (3) (2007).
[16] V. Gnielinski, New equation for heat and mass transfer in turbulent pipe and channel flow, Int. J. Chem. Eng. 16 (1976) 359–368.
[17] C.C. Wang, J.S. Liaw, B.C. Yang, Air side performance of herringbone wavy fin-and-tube heat exchangers – data with larger diameter tube, Int. J. Heat Mass Transfer 54 (2011) 1024–1029.
[18] P. Pongsoi, S. Pikulkajorn, C.C. Wang, S. Wongwises, Effect of number of tube rows on the air-side performance of crimped spiral fin-and-tube heat exchanger with a multipass parallel and counter cross-flow configuration, Int. J. Heat Mass Transfer 55 (2012) 1403–1411.

[19] C.S. An, D.H. Choi, Analysis of heat-transfer performance of cross-flow fin-tube heat exchangers under dry and wet conditions, Int. J. Heat Mass Transfer 55 (2012) 1496–1504.
[20] Y. Chang, M. Kim, Modelling and performance simulation of gas cooler for CO2 heat pump system, in: Proc. International Refrigeration and Air Conditioning Conference, Purdue University, 2006, paper 764.
[21] M.M.A.B. Bhutta, N. Hayat, M.H. Bashir, A.R. Khan, CFD applications in various heat exchangers design: a review, Appl. Therm. Eng. 32 (2012) 1–12.
[22] W. Yaïci, M. Ghorab, E. Entchev, 3D CFD analysis of the effect of inlet air flow maldistribution on the fluid flow and heat transfer performances of plate-fin-and-tube laminar heat exchangers, Int. J. Heat Mass Transfer 74 (2014) 490–500.
[23] V. Singh, O. Abdelaziz, V. Aute, R. Radermacher, Simulation of air-to-refrigerant fin-and-tube heat exchanger with CFD – based air propagation, Int. J. Refrig. 34 (2011) 1883–1897.
[24] J. Muñoz, A. Abánades, Analysis of internal helically finned tubes for parabolic trough design by CFD tools, Appl. Energy 88 (2011) 4139–4149.
[25] L. Sun, C.L. Zhang, Evaluation of elliptical finned-tube heat exchanger performance using CFD and response surface methodology, Int. J. Therm. Sci. 75 (2014) 45–53.
[26] H. Bilirgen, S. Dunbar, E.K. Levy, Numerical modelling of finned heat exchangers, Appl. Therm. Eng. 61 (2013) 278–288.
[27] B.L. Gowreesunker, S.A. Tassou, Effectiveness of CFD simulation for the performance prediction of phase change building boards in the thermal environment control of indoor spaces, Build. Environ. 59 (2013) 612–625.
[28] ANSYS FLUENT User's guide, Release 13.0, 2013, p. 699.
[29] F-Chart Software. EES (engineering equation solver); 2014, <http://www.fchart.com>.